A PARAMETERIZATION MODEL FOR CALCULATION OF VERTICAL FLUXES OF MOMENTUM DUE TO TERRAIN INDUCED GRAVITY WAVES

By William G. Collins

SMHI Rapporter

METEOROLOGI OCH KLIMATOLOGI

Nr RMK 5 (1976)

SVERIGES METEOROLOGISKA OCH HYDROLOGISKA INSTITUT

A PARAMETERIZATION MODEL FOR CALCULATION OF VERTICAL FLUXES OF MOMENTUM DUE TO TERRAIN INDUCED GRAVITY WAVES

By William G. Collins

SMHI Rapporter

METEOROLOGI OCH KLIMATOLOGI

Nr RMK 5 (1976)

SVERIGES METEOROLOGISKA OCH HYDROLOGISKA INSTITUT

Norrköping 1976

A PARAMETERIZATION MODEL FOR CALCULATION OF VERTICAL FLUXES OF MOMENTUM DUE TO TERRAIN INDUCED GRAVITY WAVES.

By William G. Collins

Summary

Various sources of information indicate vertical fluxes of mountain induced wave momentum to be on the order of several tenths of a Pascal over mountaineous terrain. The implied wind tendencies in layers of wave absorption in typical situations are several meters per second per day. On the basis of the size of this probable effect, a parameterization model has been developed to calculate the momentum fluxes within the framework of a large-scale numerical weather prediction model. The calculation model assumes a continuous linear wind profile as well as constant stability within each layer. The hydrostatic assumption is made for the total motion. The vertical velocities and resultant vertical momentum fluxes are caused by the air being forced over the topography. For this model, the individual spectral elements of the terrain height are not important. Rather, an integral over the elements is used as the forcing function which determines the momentum flux magnitude. This forcing function must be determined as a function of horizontal direction for each large-scale grid box. Sample calculations are given which illustrate the results possible from the parameterization model.

Sammanfattning

Olika källor visar att det vertikala flödet av impulsmoment beroende på gravitationsvågor kan uppgå till flera tiondels pascal över bergstrakter. De därmed sammanhängande vindtendenserna är flera m/s per dag under typiska förhållanden. Beroende på storleken av denna effekt har en metod utvecklats för att parameterisera detta flöde inom ramen för en storskalig numerisk prognosmodell. Beräkningsmodellen arbetar med en kontinuerlig, och inom varje skikt lineär vindprofil och en konstant statisk stabilitet i varje skikt. Den nedre randen i varje storskalig gridbox kommer bara in som en funktion av topografin i olika riktningar. Några testfall visar vilka resultat parameteriseringsmodellen kan ge.

I Introduction.

The nature of the vertical propogation of momentum by induced gravity waves was probably first reported by Eliassen and Palm (1960). They showed that in the absence of critical layers, layers in which the component wind velocity was the same as the wave velocity, the momentum flux will be constant with height. The earth's rotation was found later to be of some importance, but this complication can usually be neglected. What Eliassen and Palm did not do, however, was to make an estimate of the magnitude of the momentum flux. Nor did they determine what happened at a critical layer.

The conditions at a critical layer have been investigated by several authors, e.g. Blumen (1965), Bretherton (1966, 1969), Booker and Bretherton (1967), Hines and Reddy (1967), and Jones (1967). Nonlinear theories have been advanced by Benny and Bergeron (1969), Kelly and Maslowe (1970), and Maslowe (1972). Additional critical layer characteristics have been determined by Tanaka (1975). Basically, they find that the momentum is absorbed by the mean flow precisely at the critical level. In this way, momentum is transported vertically from the surface, passes through possibly deep layers without affecting them, but changes the mean flow at the lowest critical layer.

The magnitude of the total vertical flux of momentum was investigated by White (1949) and Newton (1971) by calculating the torque produced by topography upon the atmosphere due to pressure differences between the east and west faces of mountain ranges. They found the mean zonal stress from the torques to be of the order of .02 Pascals, which is about 1/5 that due to the surface frictional stress. But since significant topography in the Northern Hemisphere middle latitudes occupies about 15-20 % of the total area, this corresponds to about .1 Pascal in mountaineous regions. Therefore, the total effect upon the atmosphere in mountaineous regions may be expected to be of the same order of magnitude as the surface frictional

stresses. The way the stress affects the atmosphere is entirely different, however.

The calculations of White and Newton utilize only conventional data and may represent a lower limit to the size of the total momentum flux. This is illustrated by a theoretical calculation of Bretherton's (1969). Using detailed information about the topography in Wales, and a radiosonde sounding, he calculated a wave drag of .4 Pascals in a 19 m/s gradient wind.

Observations by aircraft at NCAR further substantiate the magnitude of the momentum fluxes. Measurements over the Rockies give values from .5 to 1 Pascal. In one case the momentum flux was found to decrease to zero in a critical layer between 12 and 15 kilometer's height.

Momentum fluxes the size of those calculated and observed can give appreciable tendencies to the winds at levels where the fluxes are dissipated. In order to see the possible effect upon the development of atmospheric variables, the NCAR global circulation model has been integrated with the inclusion of a wave drag of .7 Pa over an area corresponding the Rocky Mountains, with the flux vanishing between 12 and 15 km. Comparison between 96 hr forecasts with and without the momentum flux showed a maximum zonal reduction in wind speed of -1.6 m/s and a maximum wind reduction of -8 m/s at jet level.

Obeservations, theoretical studies, and the numerical experiment just described all point to the importance of the vertical flux of wave momentum upon the winds aloft. This paper describes a parameterization suitable for use within a large-scale numerical weather prediction model. First, the way in which the problem is posed within the framework of a large-scale forecast model will be described. Next, the numerical model used for the parameterization will be described. And finally some results will be given.

II Setting Up the Problem Within the Framework of a Large-scale Numerical Weather Prediction Model.

For most purposes it is not important to be precise about the meaning of grid-point values within a large-scale numerical weather prediction (NWP) model. However, we wish to separate the effects calculated by a large-scale model from those which we will added as sub-grid-scale contributions. Therefore, it is important to make the distinction between large-scale grid-point values and the sub-grid-scale deviations clear.

We begin by defining what is meant by large-scale. Consider a region, divided by a rectangular grid. Let (x,y) be the coordinates of the center of a grid box, and let Δx, Δy be its dimensions. Then we define

$$\overline{()} = ()_o = \int_{y-\frac{\Delta y}{2}}^{y+\frac{\Delta y}{2}} \int_{x-\frac{\Delta x}{2}}^{x+\frac{\Delta x}{2}} () \, dx \, dy \qquad (1)$$

where () stands for any variable, subcript "o" stands for large-scale, and the overbar will be used to refer to the operator on the righthand side of (1). It is noted that $()_o$ is a constant, which varies only from one box to another, and perhaps in time.

Now we define what is meant by finite differences of the large-scale. They are merely differences of large-scale values, where distances as needed are calculated from the centers of boxes. Total fields may be represented as

$$() = ()_o + ()' \qquad (2)$$

This equation also serves to define the small-scale, ()'. We will now develop the equations of motion for both the large-scale and small-scale. We begin by giving the equations for the total motion fields.

$$\frac{\partial u}{\partial t} + u\frac{\partial u}{\partial x} + v\frac{\partial u}{\partial y} + w\frac{\partial u}{\partial z} - fv + \frac{1}{\rho}\frac{\partial p}{\partial x} = 0 \qquad (3)$$

$$\frac{\partial v}{\partial t} + u\frac{\partial v}{\partial x} + v\frac{\partial v}{\partial y} + w\frac{\partial v}{\partial z} + fu + \frac{1}{\rho}\frac{\partial p}{\partial y} = 0 \qquad (4)$$

$$g + \frac{1}{\rho}\frac{\partial p}{\partial z} = 0 \qquad (5)$$

$$\frac{\partial \rho}{\partial t} + u\frac{\partial \rho}{\partial x} + v\frac{\partial \rho}{\partial y} + w\frac{\partial \rho}{\partial z} + \rho\left(\frac{\partial u}{\partial x} + \frac{\partial v}{\partial y} + \frac{\partial w}{\partial z}\right) = 0 \qquad (6)$$

$$\frac{\partial p}{\partial t} + u\frac{\partial p}{\partial x} + v\frac{\partial p}{\partial y} + w\frac{\partial p}{\partial z} + \gamma\frac{p}{\rho}\left(\frac{\partial u}{\partial x} + \frac{\partial v}{\partial y} + \frac{\partial w}{\partial z}\right) = 0 \qquad (7)$$

It is assumed that the hydrostatic equation holds for the total motion. This places a lower limit to the scale of motions that can be considered, around 5 km, but allows fairly accurate representation of the waves of most interest, those with wavelengths 10 km and greater.

We continue the development, using the x-momentum equation, eqn. (3) as an example. Introducing (2) into (3) gives

$$\frac{\partial(u_0+u')}{\partial t} + (u_0+u')\frac{\partial(u_0+u')}{\partial x} + (v_0+v')\frac{\partial(u_0+u')}{\partial y} +$$

$$+ (w_0+w')\frac{\partial(u_0+u')}{\partial z} - f(v_0+v') + \frac{1}{\rho_0+\rho'}\frac{\partial(p_0+p')}{\partial x} = 0 \qquad (8)$$

Grouping terms gives

$$\frac{\partial u_0}{\partial t} + u_0\frac{\partial u_0}{\partial x} + v_0\frac{\partial u_0}{\partial y} + w_0\frac{\partial u_0}{\partial z} - fv_0 + \frac{1}{\rho_0}\frac{\partial p_0}{\partial x}$$

$$+ \frac{\partial u'}{\partial t} + u_0\frac{\partial u'}{\partial x} + v_0\frac{\partial u'}{\partial y} + w_0\frac{\partial u'}{\partial z} + w'\frac{\partial u_0}{\partial z} - fv' + \frac{1}{\rho_0}\frac{\partial p'}{\partial x}$$

$$+ u'\frac{\partial u_0}{\partial x} + u'\frac{\partial u'}{\partial x} + v'\frac{\partial u_0}{\partial y} + v'\frac{\partial u'}{\partial y} + w'\frac{\partial u'}{\partial z}$$

$$- \frac{\rho'}{\rho_0}\frac{1}{\rho_0+\rho'}\frac{\partial(p_0+p')}{\partial x} = 0 \qquad (9)$$

Let us perform the operation $\bar{()}$ on this equation. It is noted that

$$\overline{()}' = 0$$

$$\overline{()_o()_o} = ()_o()_o \qquad (10)$$

$$\overline{()_o} = ()_o$$

We get

$$\frac{\partial u_0}{\partial t} + u_0\frac{\partial u_0}{\partial x} + v_0\frac{\partial u_0}{\partial y} + w_0\frac{\partial u_0}{\partial z} - fv_0 + \frac{1}{\rho_0}\frac{\partial p_0}{\partial x} +$$

$$+ \overline{u'\frac{\partial u'}{\partial x}} + \overline{v'\frac{\partial u'}{\partial y}} + \overline{w'\frac{\partial u'}{\partial z}} - \overline{\frac{\rho'}{\rho_0}\frac{1}{\rho_0+\rho'}\frac{\partial(p_0+p')}{\partial x}} = 0 \quad (11)$$

The horizontal differentials of the large-scale quantities must be interpreted as finite differences, as discussed earlier. Eqn. (11) represents the forecast equation for the large-scale variable, u_o. It involves the Reynolds stressterms. It is these terms, with appropriate approximations, that the small-scale model will calculate. The equations for the small-scale are obtained by subtracting the equations for the large-scale from the total equations. For u' we get

$$\frac{\partial u'}{\partial t} + u_0\frac{\partial u'}{\partial x} + v_0\frac{\partial u'}{\partial y} + w_0\frac{\partial u'}{\partial z} + w'\frac{\partial u_0}{\partial z} - fv' + \frac{1}{\rho_0}\frac{\partial p'}{\partial x} +$$

$$+ \left(u'\frac{\partial u'}{\partial x} - \overline{u'\frac{\partial u'}{\partial x}}\right) + \left(v'\frac{\partial u'}{\partial y} - \overline{v'\frac{\partial u'}{\partial y}}\right) + \left(w'\frac{\partial u'}{\partial z} - \overline{w'\frac{\partial u'}{\partial z}}\right)$$

$$- \left(\frac{\rho'}{\rho_0}\frac{1}{\rho_0+\rho'}\frac{\partial(p_0+p')}{\partial x} - \overline{\frac{\rho'}{\rho_0}\frac{1}{\rho_0+\rho'}\frac{\partial(p_0+p')}{\partial x}}\right) = 0 \qquad (12)$$

In order to solve (12) we make the assumption of linearization. This is an accurate assumption with regard to p and ρ but is less accurate for u and v. In any case, the terms on the last line of (12) are extremely small. By linearizing the equations, the first terms in the parentheses are neglected. We finally need to consider the second terms in the parentheses, namely

$$-R \equiv \overline{u'\frac{\partial u'}{\partial x}} + \overline{v'\frac{\partial u'}{\partial x}} + \overline{w'\frac{\partial u'}{\partial z}} =$$

$$= \overline{\frac{\partial u'^2}{\partial x}} + \overline{\frac{\partial u'v'}{\partial y}} + \overline{\frac{\partial u'w'}{\partial z}} - \overline{u'\left(\frac{\partial u'}{\partial x} + \frac{\partial v'}{\partial y} + \frac{\partial w'}{\partial z}\right)} \qquad (13)$$

Since $\overline{()'} = 0$, we expect $\overline{\frac{\partial u'^2}{\partial x}}$ and $\overline{\frac{\partial u'v'}{\partial y}}$ to vanish on the average. Also, the average divergence must be small. We are left with $\overline{\frac{\partial u'w'}{\partial z}}$ as the most significant term. It is noted that the same terms, -R, are found in the large-scale equations but with the opposite sign. The same approximations apply to the terms there. With the approximations discussed here, the equation for u' becomes

$$\frac{\partial u'}{\partial t} + u_0\frac{\partial u'}{\partial x} + v_0\frac{\partial u'}{\partial y} + w_0\frac{\partial u'}{\partial z} + w'\frac{\partial u_0}{\partial z} - fv' +$$

$$+ \frac{1}{\rho_0}\frac{\partial p'}{\partial x} - \frac{\partial}{\partial z}\overline{(u'w')} = 0 \qquad (14)$$

The small-scale model will be used in such a manner that the regions of momentum flux divergence are excluded from the regions of calculation. The method of obtaining the momentum flux divergences, when they occur is discussed in section VI. Such regions occur because of critical layers and possibly other physical processes. At all other places, as required by theory, $\overline{\frac{\partial u'w'}{\partial z}}$ vanishes.

Additional approximations will be made to the small-scale equations so they can be solved more economically. Time-dependent calculation indicate that the small-scale gravity waves adjust rather rapidly to the large-scale conditions. Therefore, the small-scale has been assumed to be steady during a large-scale timestep. Further, for the scale of motions considered, the Rossby No. is of the order of 1 or larger, allowing the neglect of the Coriolis terms in the small-scale equations.

With these approximations, as well as those discussed in the derivation of the u'-equation, the small-scale equations are now given.

$$u_0\frac{\partial u'}{\partial x} + v_0\frac{\partial u'}{\partial y} + w'\frac{du_0}{dz} + \frac{1}{\rho_0}\frac{\partial p'}{\partial x} = 0 \tag{15}$$

$$u_0\frac{\partial v'}{\partial x} + v_0\frac{\partial v'}{\partial y} + w'\frac{dv_0}{dz} + \frac{1}{\rho_0}\frac{\partial p'}{\partial y} = 0 \tag{16}$$

$$g\frac{\rho'}{\rho_0} + \frac{1}{\rho_0}\frac{\partial p'}{\partial z} = 0 \tag{17}$$

$$u_0\frac{\partial \rho'}{\partial x} + v_0\frac{\partial \rho'}{\partial y} + w'\frac{d\rho_0}{dz} + \rho_0\left(\frac{\partial u'}{\partial x} + \frac{\partial v'}{\partial y} + \frac{\partial w'}{\partial z}\right) = 0 \tag{18}$$

$$u_0\frac{\partial p'}{\partial x} + v_0\frac{\partial p'}{\partial y} + w'\frac{dp_0}{\partial z} + \gamma\frac{p_0}{\rho_0}\left(\frac{\partial u'}{\partial x} + \frac{\partial v'}{\partial y} + \frac{\partial w'}{\partial z}\right) = 0 \tag{19}$$

and the large-scale equations are

$$\frac{\partial u_0}{\partial t} + u_0\frac{\partial u_0}{\partial x} + v_0\frac{\partial u_0}{\partial y} + w_0\frac{\partial u_0}{\partial z} - fv_0 + \frac{1}{\rho_0}\frac{\partial p_0}{\partial x} + \frac{\partial \overline{u'w'}}{\partial z} = 0 \tag{20}$$

$$\frac{\partial v_0}{\partial t} + u_0\frac{\partial v_0}{\partial x} + v_0\frac{\partial v_0}{\partial y} + w_0\frac{\partial v_0}{\partial z} + fu_0 + \frac{1}{\rho_0}\frac{\partial p_0}{\partial y} + \frac{\partial \overline{v'w'}}{\partial z} = 0 \tag{21}$$

$$g + \frac{1}{\rho_0}\frac{\partial p_0}{\partial z} = 0 \tag{22}$$

$$\frac{\partial \rho_0}{\partial t} + u_0\frac{\partial \rho_0}{\partial x} + v_0\frac{\partial \rho_0}{\partial y} + w_0\frac{\partial \rho_0}{\partial z} + \rho_0\left(\frac{\partial u_0}{\partial x} + \frac{\partial v_0}{\partial y} + \frac{\partial w_0}{\partial z}\right) = 0 \tag{23}$$

$$\frac{\partial p_0}{\partial t} + u_0\frac{\partial p_0}{\partial x} + v_0\frac{\partial p_0}{\partial y} + w_0\frac{\partial p_0}{\partial z} + \gamma\frac{p_0}{\rho_0}\left(\frac{\partial u_0}{\partial x} + \frac{\partial v_0}{\partial y} + \frac{\partial w_0}{\partial z}\right) = 0 \tag{24}$$

The actual form of the large-scale equations will differ depending upon the model, and additional physical processes may be included, but by and large, (20) to (24) represent well the equations used in many operational

NWP models. What is most important to see is which terms are added by the influence of momentum flux by small-scale gravity waves.

III Solution of Small-scale Equations.

The small-scale equations are solved in the conventional manner. First, an equation is obtained for the vertical velocity by eliminating the other variables between the equations. Then the equation is separated by assuming horizontal periodicity. This gives

$$\frac{d^2\hat{w}_\ell}{dz^2} + m_\ell^2\,\hat{w}_\ell = 0 \qquad (25)$$

where ℓ is an index relating to the model layer,

$$m_\ell^2 = \frac{N_\ell^2}{u_\ell^2}\ ;\ N_\ell = \text{Brunt Vaisala frequency} \qquad (26)$$

and

$$w'(X,\phi,z) = \rho_0^{-1/2}\ \mathrm{Re}\sum_{j=1}^{N}\hat{w}_\ell(Kj,\phi,z)e^{iKjX},\ Kj=\frac{2\pi j}{\Delta x} \qquad (27)$$

X is the distance in the direction ϕ, Re means "real part", and Δx is the grid increment of the large-scale model.

Equation (25) is solved with a vertical structure governed by the NWP model in which these calculations are made. The structure is shown in Figure 1 for N layers. The wind is assumed to be continuous and to have constant shear within each layer. The stability is assumed to be constant within each layer. With these assumptions, the solution within each layer is given by Klemp and Lilly (1975) as

$$\hat{w}_\ell(\delta_\ell,\phi) = e^{\alpha_\ell\delta_\ell/2}(a_\ell(\phi)\cos\mu_\ell\delta_\ell + b_\ell(\phi)\sin\mu_\ell\,\delta_\ell)$$
$$\ell=1,2,..,N \qquad (28)$$

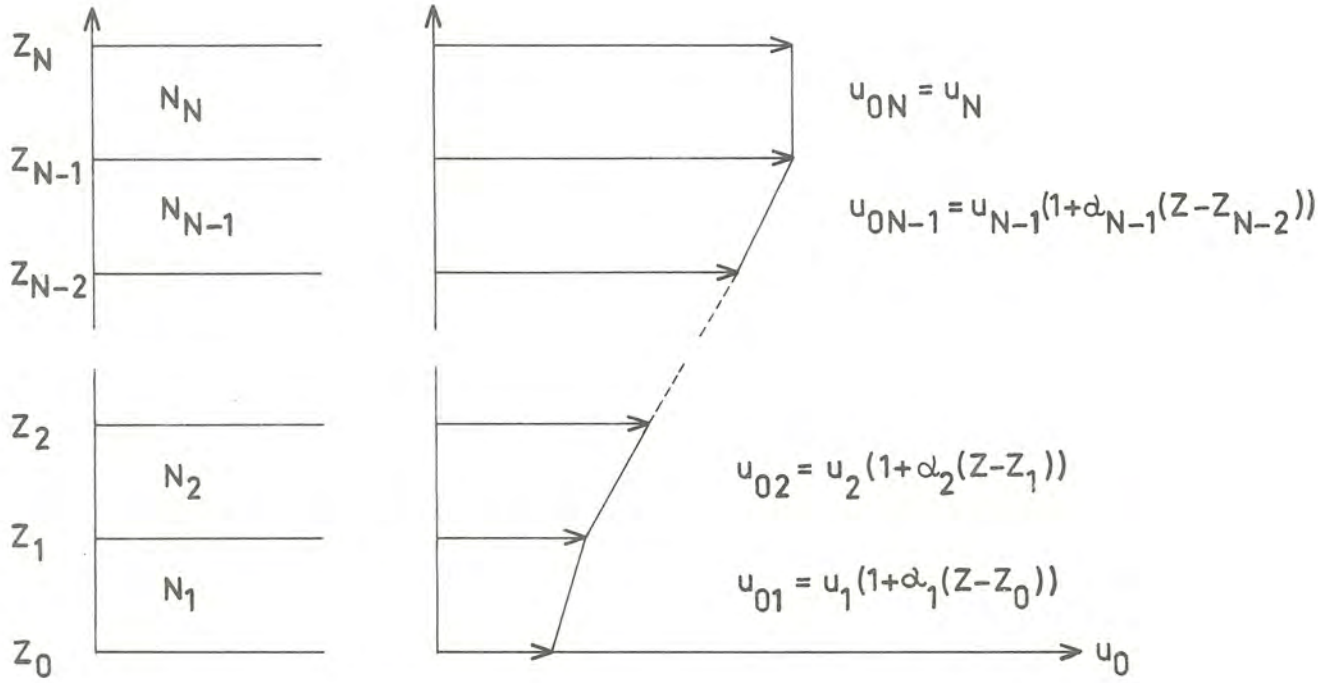

Figure 1. Model vertical structure

where

$$m_\ell^2 = \frac{N_\ell^2}{u_\ell^2(1+\alpha_\ell(z-z_{\ell-1}))^2}, \quad u_\ell \text{ is in direction } \phi \tag{29}$$

$$\alpha_\ell = \frac{1}{u_\ell}\frac{\partial u_\ell}{\partial z} \tag{29a}$$

$$N_\ell^2 = \frac{g}{\theta_\ell}\frac{\partial \theta_\ell}{\partial z} \tag{30}$$

$$\delta_\ell = \frac{1}{\alpha_\ell}\ln\left[1+\alpha_2(z-z_{\ell-1})\right] \tag{31}$$

$$\mu_\ell^2 = \frac{N_\ell^2}{u_\ell^2} - \frac{\alpha_\ell^2}{4} = \ell_\ell^2(1-\frac{1}{4R_\ell}) \tag{32}$$

where ℓ_ℓ is the Scorer parameter and R_ℓ is the Richardson No.

Equation (28) involves the two constants a_ℓ and b_ℓ for each layer. These constants are to be determined by the boundary conditions and the matching conditions between layers. The matching conditions require the continuity of the pressure and vertical velocity at layer boundaries. Equations (15) to (19) may be used to obtain the following equation for the pressure.

$$-iKj\hat{p}_\ell = u_{0\ell}\hat{w}_{\ell_z} + u_{0\ell}(-\frac{N_\ell}{2g}\frac{c_p}{R} + \frac{u_{0\ell_z}}{u_{0\ell}})\hat{w}_\ell$$

$$\approx -u_{0\ell}\left[\hat{w}_{\ell_z} - \frac{u_{0\ell_z}}{u_{0\ell}}\hat{w}_\ell\right], \text{ where } ()_z = \frac{\partial}{\partial z}(). \tag{33}$$

Continuity of p at layer boundaries therefore requires

$$\hat{w}_{\ell+1_z} - \frac{u_{0\ell+1_z}}{u_{0\ell+1}}\hat{w}_{\ell+1} = \hat{w}_{\ell_z} - \frac{u_{0\ell_z}}{u_{0\ell+1}}\hat{w}_\ell \tag{34}$$

where the fact that the basic wind is continuous and equal to $u_{0\ell+1}$ at the boundary, has been used. But since $\hat{w}_\ell = \hat{w}_{\ell+1}$ by the continuity of w, this can be written

$$\hat{w}_{\ell_z} = \hat{w}_{\ell+1_z} - (\alpha_{\ell+1} - \alpha_\ell \frac{u_{0_\ell}}{u_{0_{\ell+1}}})\hat{w}_\ell \tag{35}$$

The lower boundary condition states that the air must flow smoothly over the topography, with no frictional losses. The ground profile may be given by

$$\zeta_0(X,\phi) = \sum_{j=0}^{\infty} H_1(Kj,\phi)e^{iKjX} \tag{36}$$

where

$$H_1(Kj,\phi) = \frac{2}{\Delta X}\int_{X_0-\frac{\Delta X}{2}}^{X_0+\frac{\Delta X}{2}} \zeta_0(X,\phi)e^{-iKjX}dX, \quad j=1,2,.. \tag{37}$$

Then the lower boundary condition (linearized) is

$$w'(z=0) = u_1\frac{d\zeta_0}{dX}$$

$$= u_1 \mathrm{Re} \sum_{j=1}^{N} iKj\, H_1(Kj,\phi)e^{iKjX} \tag{38}$$

In terms of $\hat{w}$, this condition is

$$\hat{w}(Kj,0,\phi) = \rho_0^{1/2}\, u_1 Kj H_1(Kj,\phi) \tag{39}$$

It will be convenient to calculate using

$$w_\ell^*(z,\phi) = \hat{w}_\ell(Kj,z,\phi)/iKj H_1(Kj,\phi) \tag{40}$$

since w_ℓ^* is independent of Kj.

The upper boundary condition is formulated to allow any momentum flux approaching the boundary to flow through the boundary unimpeded. The condition used is usually called the radiation condition. It is normally applied at the top of the model atmosphere, but if a critical layer is present, or if other physical processes are expected to give momentum flux divergence, the boundary condition is applied at the layer boundary just below. The momentum flux approaching this level is assumed to be absorbed at this level, but the resulting

wind tendencies are spread through the model layer in which the level occurs.

With the matching conditions and boundary conditions as given by (35) and (37), then (28) results in algebraic equations with the same number of equations as unknowns. The solution method used takes advantage of the form of the equations and their linearity to solve them more efficiently than by matrix inversion.

IV Solution for Vertical Momentum Fluxes.

The small-scale equations have been used to solve for the vertical velocity. They may equally well be used to obtain the horizontal velocity, pressure, or density. In order to calculate the vertical momentum flux, a relationship between the vertical and horizontal velocities is needed. It may be found from (15) to (19). That relationship is

$$\hat{u}_\ell(Kj,z,\phi) = \frac{i}{Kj}\left[\frac{d\hat{w}_\ell(Kj,z,\phi)}{dz} + \frac{R\,N_i}{2gcp}\hat{w}_\ell(Kj,z,\phi)\right] \quad (41)$$

This may be used to calculate the average momentum flux:

$$\begin{pmatrix}\rho_0\overline{u'w'}\\ \rho_0\overline{v'w'}\end{pmatrix} = 2\int_{\phi_0-\pi/2}^{\phi_0+\pi/2}\frac{1}{\Delta X}\int_{X_0-\frac{\Delta X}{2}}^{X_0+\frac{\Delta X}{2}}\rho_0 u'w'dX\begin{pmatrix}\cos\phi\\ \sin\phi\end{pmatrix}d\phi$$

$$= -\frac{i}{2}\int_{\phi_0-\pi/2}^{\phi_0+\pi/2}A(\phi)(w^*w_z^{*c}-w^{*c}w_z^*)\begin{pmatrix}\cos\phi\\ \sin\phi\end{pmatrix}d\phi \quad (42)$$

where u' is in the x-direction, v' is in the y-direction, ϕ is measured with respect to the x-direction, ϕ_c is the direction of the surface wind, c refers to the complex conjugate, and

$$A(\phi) = A(\Delta X,N,\phi) = \sum_{j=1}^{N} Kj\,H_{,j}\,H_{,j}^{c}$$

$$= \sum_{j=1}^{N} \frac{2\pi j}{\Delta X} H_{,j} H_{,j}^{c} \tag{43}$$

The topography enters only through this sum over the mountain spectrum.

V Momentum Flux Within Model Layers.

Eliassen and Palm (1960) showed for a linear model, and Lindzen (1973) has extended the result to a non-linear Boussinesq fluid that the vertical flux of horizontal momentum by gravity waves in a particular direction must be constant with height, in the absence of absorption and layers where the wind speed vanishes in this direction. We will show now that the gravity wave model given here satisfies these requirements, and further, that the vertical flux of momentum remains constant across layer boundaries. The vertical flux of horizontal momentum in the direction of u, and averaged over a horizontal wavelength, is given by

$$\rho_0 \overline{u'w'} \propto w_z^{*c} w^* - w_z^* w^{*c}$$

$$= \left(\frac{\partial w^*}{\partial \delta} \frac{\partial \delta_\ell}{\partial z}\right)^c w^* - \left(\frac{\partial w^*}{\partial \delta} \frac{\partial \delta_\ell}{\partial z}\right) w^{*c}$$

$$= \frac{\partial \delta_\ell}{\partial z} \left(\frac{\partial w^*}{\partial \delta}^c w^* - \frac{\partial w^*}{\partial \delta} w^{*c}\right) \tag{44}$$

$$= \frac{\partial \delta_\ell}{\partial z} \left\{\left[\frac{\alpha_\ell}{2} w^{*c} + \mu_i (-a_\ell^c \sin\mu\delta + b_\ell^c \cos\mu\delta) e^{\alpha_\ell \delta_\ell/2}\right] \cdot \right.$$

$$(a_\ell \cos\mu\delta + b_\ell \sin\mu\delta) e^{\alpha_\ell \delta_\ell/2}$$

$$- \left[\frac{\alpha_\ell}{2} w^* + \mu_\ell (-a_\ell \sin\mu\delta + b_\ell \cos\mu\delta) e^{\alpha_\ell \delta_\ell/2}\right] \cdot$$

$$\left. (a_\ell^c \cos\mu\delta + b_\ell^c \sin\mu\delta) e^{\alpha_\ell \delta_\ell/2}\right\}$$

$$= \mu_\ell (a_\ell b_\ell^c - a_\ell^c b_\ell) \tag{45}$$

Since all these factors are constant within a layer, so is $\rho_0\overline{u'w'}$. Next, we will show that the matching conditions conserve the vertical momentum flux. We use the matching conditions, (35), and $w^*_{\ell+1} = w^*_\ell$ to show the equivalence. We have

$$\rho_0\overline{u'w'} \propto w^{*c}_z w^* - w^*_z w^{*c}$$

$$= \left[w^{*c}_{\ell+1_z} - (\alpha_{\ell+1} - \alpha_\ell \frac{u_\ell}{u_{\ell+1}}) w^{*c}_\ell\right] w^*_\ell -$$

$$\left[w^*_{\ell+1_z} - (\alpha_{\ell+1} - \alpha_\ell \frac{u_\ell}{u_{\ell+1}}) w^*_\ell\right] w^{*c}_\ell$$

$$= w^{*c}_{\ell+1_z} w^*_\ell - w^*_{\ell+1_z} w^{*c}_\ell$$

$$= w^{*c}_{\ell+1_z} w^*_{\ell+1} - w^*_{\ell+1_z} w^{*c}_{\ell+1} \qquad (46)$$

Thus, the momentum flux is equal within the two layers.

VI Processes Giving Momentum Flux Divergence.

The arguments of the last section show that under most circumstances, the vertical flux of horizontal momentum is constant with height. We will mow consider conditions in which this is not true, for these are the conditions in which the small-scale affects the large-scale through the terms $\overline{\frac{\partial u'w'}{\partial z}}$ and $\overline{\frac{\partial v'w'}{\partial z}}$. The expression for the vertical wavenumber in the δ-vertical coordinate will reveal two of these conditions. Equation (32) shows that the vertical wavenumber is given by

$$\mu_\ell = \left(\frac{N^2_\ell}{u^2_\ell} - \frac{\alpha^2_\ell}{4}\right)^{1/2} = \frac{1}{u_\ell}\left(N^2_\ell - \frac{(\alpha_\ell u_\ell)^2}{4}\right)^{1/2} = \ell_\ell (1 - \frac{1}{4R_\ell})^{1/2}$$

The vertical wavenumber becomes infinite if $u_\ell = 0$ or imaginary if $R_\ell \leq \frac{1}{4}$. The layered structure of the model prevents us from seeing the variation of the wavenumber within a layer, but in a continuously stratified model we expect the vertical wavenumber to become infinite

at any location where u=0. At such locations the arguments of the last section fail. The methods of determining the conditions across such layers are beyond the scope of this paper, but considerable literature exists on the subject as cited earlier. The first condition, u=0, occurs for this model at a level where the gravity wave speed is identical to the wind speed. Such a level is called a critical level. Bretherton (1969) showed that the momentum flux is reduced to practically zero across such a layer. In fact, the factor by which the momentum flux is reduced is

$$\exp\left[-2\pi(R_\ell-1/4)^{1/2}\right] \tag{47}$$

Apparently, if $R_\ell>1$, the momentum flux is greatly reduced. If, on the other hand, $R_\ell\leq\frac{1}{4}$, then turbulence will form and grow, and the waves will be destroyed by the turbulent mechanism. In any case, within a layer in which either a critical layer exists or the Richardson number is less than $\frac{1}{4}$, the momentum flux divergence is approximated in the model by

$$\frac{\partial}{\partial z}(u'w')\approx\frac{\overline{u_l'w_l'}}{z_{\ell+1}-z_\ell} \tag{48}$$

Both conditions can be diagnosed before the solution for w^* is obtained, which is fortunate, since the upper boundary condition must be changed in such cases.

Since the numerical model is unable to give directly the layers of flux divergence, it is necessary to account for them in a special manner. The procedure is to first test for locations of basic wind vanishing or $R_\ell\leq\frac{1}{4}$. In such cases, the numerical solution above such a layer would be meaningless. As a result, the upper boundary condition is applied at the first layer boundary below. And then (48) is used to calculate the flux divergence within the layer. It is appropriate at this point to make a note that recent calculations of Tanaka (1975) indicate a possible modification to the picture given here of the vertical flux of momentum

and its divergence. Their nonlinear calculations indicate a possible shuting off of the vertical flux of momentum after some time when critical layers are present. This apparently takes place in the calculations because of modification of the basic state variables by the earlier absorption of momentum near the critical layer.At present there is no way of acessing the possible importance of this machanism, so it will be ignored. It's possibility is acknowleged, however.

VII Lower Boundary Specification.

We finally get to a rather interesting and separate problem, the specification of the lower boundary form. It is noted that the lower boundary enters the calculation in only one way. In calculation of the momentum fluxes it enters as $\sum_{j=1}^{N} Kj H_{1j} H_{1j}^{c}$. Therefore, it is not necessary to know $H_1(K,\phi)$, only a sum of this height function. What would be desireable is a way of estimating this sum from gross characteristics of the topography.

Some work by Lee and Kaula (1967) and Bretherton (1969) has suggested a way of approximating the height sum. Lee and Kaula used data over the whole globe to define spherical harmonics of the terrain height. And Bretherton used terrain heights over Wales to define the Fourier spectrum of the heights. Bretherton noted that both these spectra can be given quite closely by

$$H_1(K) = \overline{H}_1 \left(\frac{Ka}{K}\right)^{\alpha}, Ka = 1\ Km^{-1}, \alpha = .75 \qquad (49)$$

and where $\overline{H}_1$ from the two data samples was similar. Bretherton remarks that the agreement must be somewhat fortuitous, especially since the range of K for the two sets of data does not overlap. But it was thought that the equation was worth further testing, particularly since its validity would provide a simple way of approximating the required height sum. Two further sets of height data have been used. The first consists of data

at 12 km intervals through Sweden between 56°N and 61°N. Three groups of data were averaged for 13°E, 14°E and 15°E. This data has been fit by least squares to

$$H_1(K) = 1.85\left(\frac{Ka}{K}\right)^{.84} \tag{50}$$

The data are shown as dots in Figure 2 and the least squares straight line fit is also shown.

The second set of data was from 1° longitude terrain heights at 45°N encircling the globe. The data are from Berkofsky and Bertoni (1960). This data fits quite well the curve

$$H_1(K) = 1.6\left(\frac{Ka}{K}\right)^{.76} \tag{51}$$

There is some overlap in the range of K of the data used to obtain (50) and (51), but the data is independent. Figure 2 shows amplitudes of the terrain spectrum that have been smoothed with respect to wavenumber, making visual linear approximation to the data easier. The linear fit, as given by (51), is also shown in the figure.

The form of these approximations to the terrain spectra could lead one to interesting speculation as to their meaning. But that is not necessary for the needs of this investigation. What is important is that we are provided with a way of approximating a sum over the mountain spectrum. What we can do is to fit (49) to the values of local heights, with α near .75, and form the appropriate sum. It is (taking α=.75)

$$A(\Delta X, M, \phi) \approx \overline{H}_1^2(\phi) Ka^{3/2} \left(\frac{\Delta X}{\pi}\right)^{1/2} \sum_{j=1}^{M} \left(\frac{1}{j}\right)^{1/2} \tag{52}$$

for $H_1(K)$ given by (49). Therefore, once Δx and M are specified, the sum depends merely upon $\overline{H}_1$. Let us see first how Δx and M are specified, and then consider the

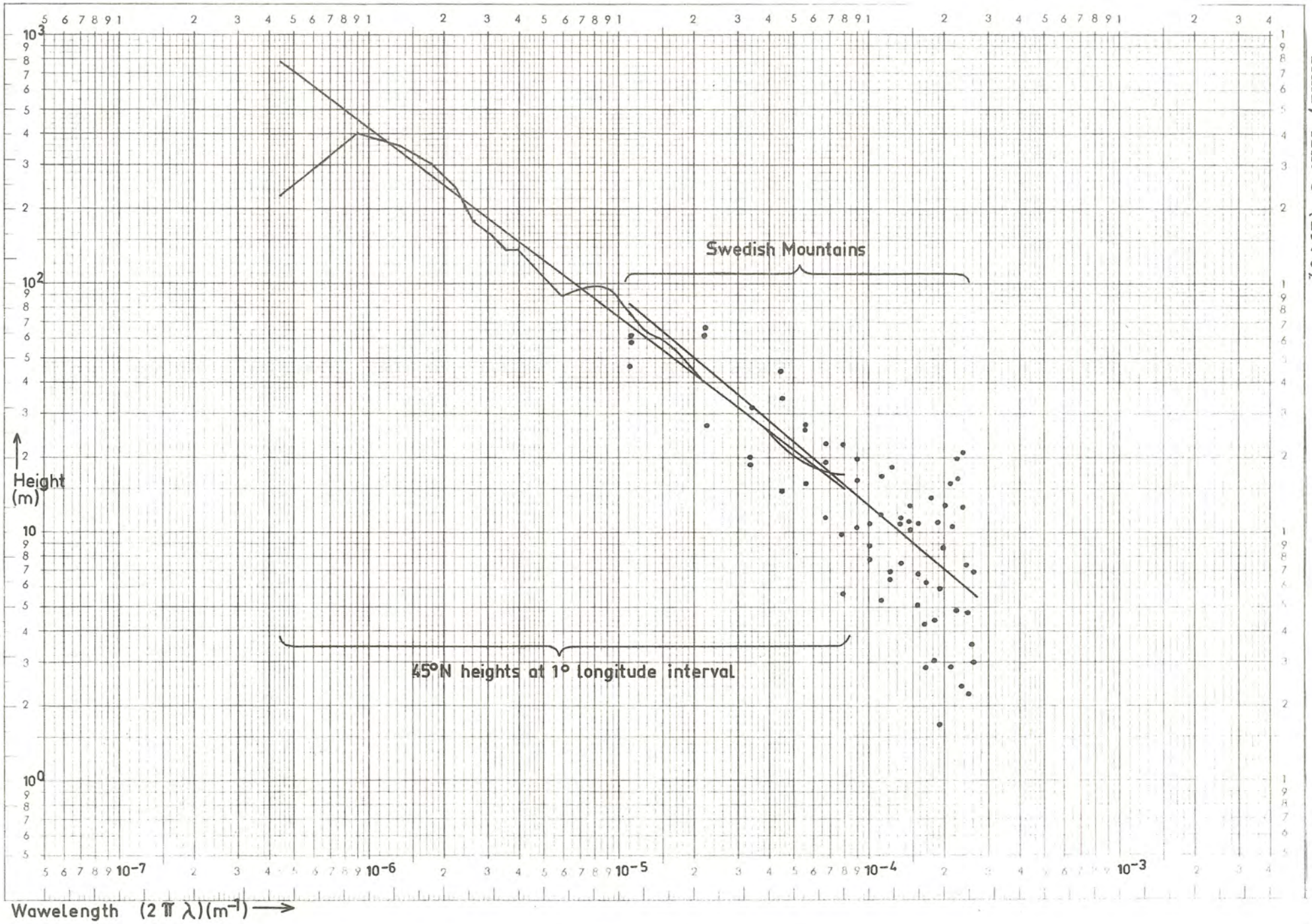

Figure 2. Mountain Height Spectra

determination of $\bar{H}_1$. First, Δx is merely the gridspacing. And M is the largest wavenumber with respect to Δx that we want to include in the calculations. In fact, if we had used the nonhydrostatic wave equation, the upper limit to M would be determined by physical principles. That limit would be

$$M = \frac{N_\ell \Delta x/\pi}{u_\ell \left[1+\alpha_\ell (z-z_\ell)\right]}$$

for any layer ℓ. For our purposes here we can merely choose a reasonable average value. Actually, the hydrostatic approximation utterly fails near this limit and we might choose M somewhat smaller. For now, let us suppose that $M = 2\Delta x/5\text{km}$. Let us suppose that $\Delta x = 278$ km, the grid-spacing of the National Meteorological Center 8-layer global model.

It remains to find a way of specifying $\bar{H}_1$, which should be a slowly varying function of postiion, since it relates to gross features of the topography, and which may also be a function of azimuth, ϕ. There seem to be several approaches to this problem. One possibility is to measure a few components of the spectrum in order to estimate $\bar{H}_1$ as a function of ϕ for each grid box.

VII Sample Two-Dimensional Solution.

A sample two-dimensional model result which illustrates the kind of actual results obtainable by this model will be shown. In the case chosen a standard atmosphere temperature sounding has been assumed. It uses average winter zonal winds at 45°N. The winds increase rather uniformly up to the lower stratosphere and then decrease above. Therefore, it has no critical level.

Figure 3 shows the solution for the real and imaginary parts of w^*. Also shown is the wind at the base of each layer. It is seen that both the amplitude and wavelength of the wave have significant changes in the vertical. The real part of w^* gives the vertical velocity above

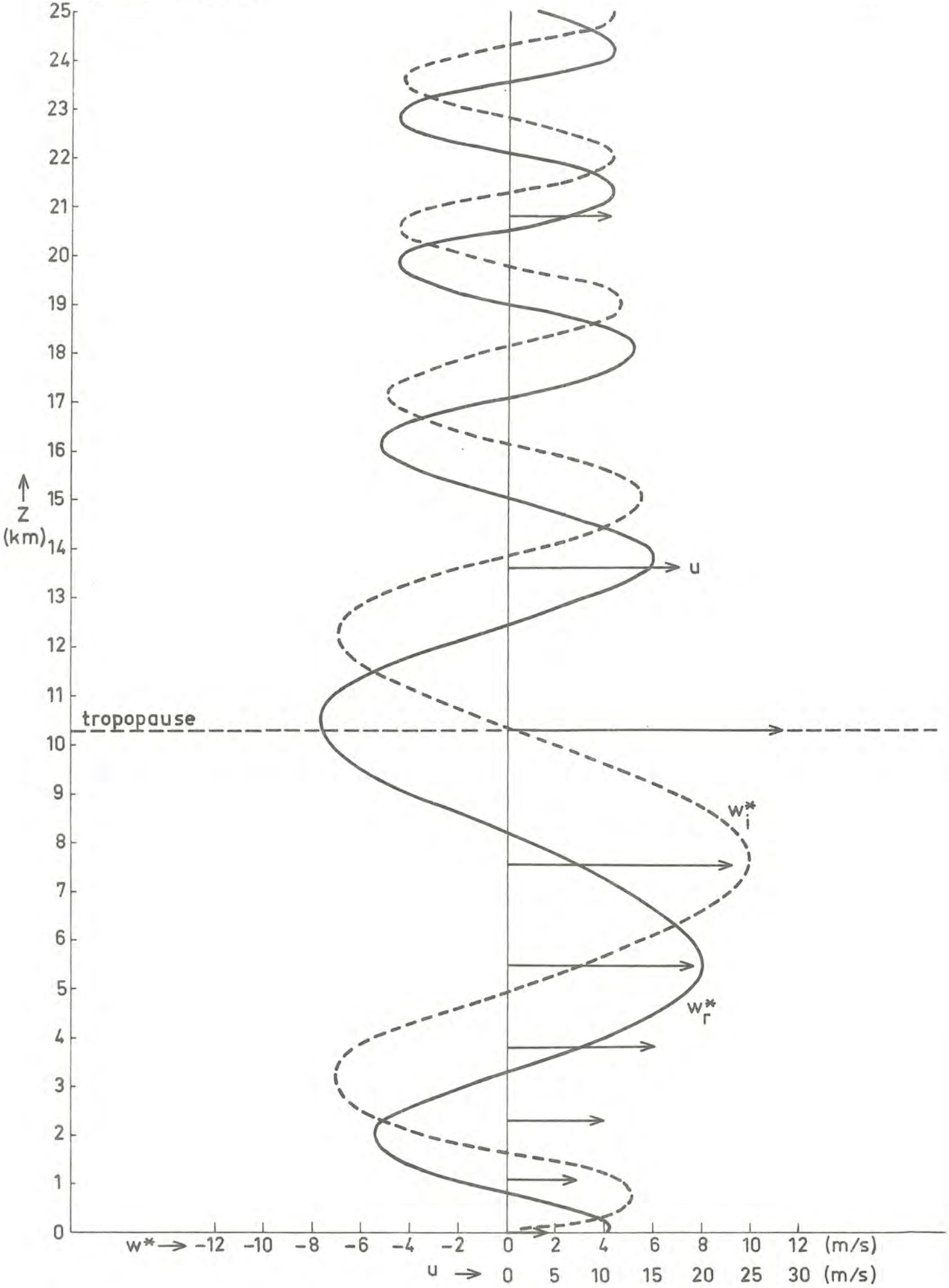

Figure 3. Solution for w*. Standard atmosphere temperatures. Average winter 45°N zonal winds.

the sinusoidal ground where the ground slope is the greatest. The slope is taken as one so that $w_r^*(0)$ has the magnitude of u_1. The imaginary part of w^* gives the vertical velocity above the ground 1/4 wavelength upstream.

Since this case shows no critical level or other mechanism of wave absorption within the troposphere or lower stratosphere, the momentum will affect the large-scale wind at even greater heights. In the absence of other effects, molecular absorption becomes important at 80 to 100 km heights. The amount by which the wind is affected would depend upon the depth of the layer through which the momentum flux drops to zero. Since such high levels are not at all modelled by operational NWP models, such effects will not be considered further. The total vertical flux of horizontal momentum was found to be -.032 Pa for an average mountain profile, using $\overline{H}_1 = 1.6$ and grid increment as suggested earlier.

VIII Sample Three-Dimensional Solution.

A case where the wind direction varies with height is shown to illustrate the results in three dimensions. This case was chosen largely at random, but is one with sufficient wind direction changes with height, so that critical levels exist over some ranges of azimuth. Figure 4 shows the wind and temperature profiles for this case. The temperatures show large stability at low levels (to about 700 mb) and in the stratosphere, with lesser stability between. The winds show veering at low levels, nearly constant direction to the tropopause, and backing above. This pattern leads to critical levels both at low and high altitudes for some azimuth angles.

Figure 5 shows both the height of critical levels and the vertical momentum flux (in arbitrary units) as a function of azimuth angle, where $\phi = 90.5^{\circ}$ is the direction of the lowest layer wind. It happens to be a west wind in this case.

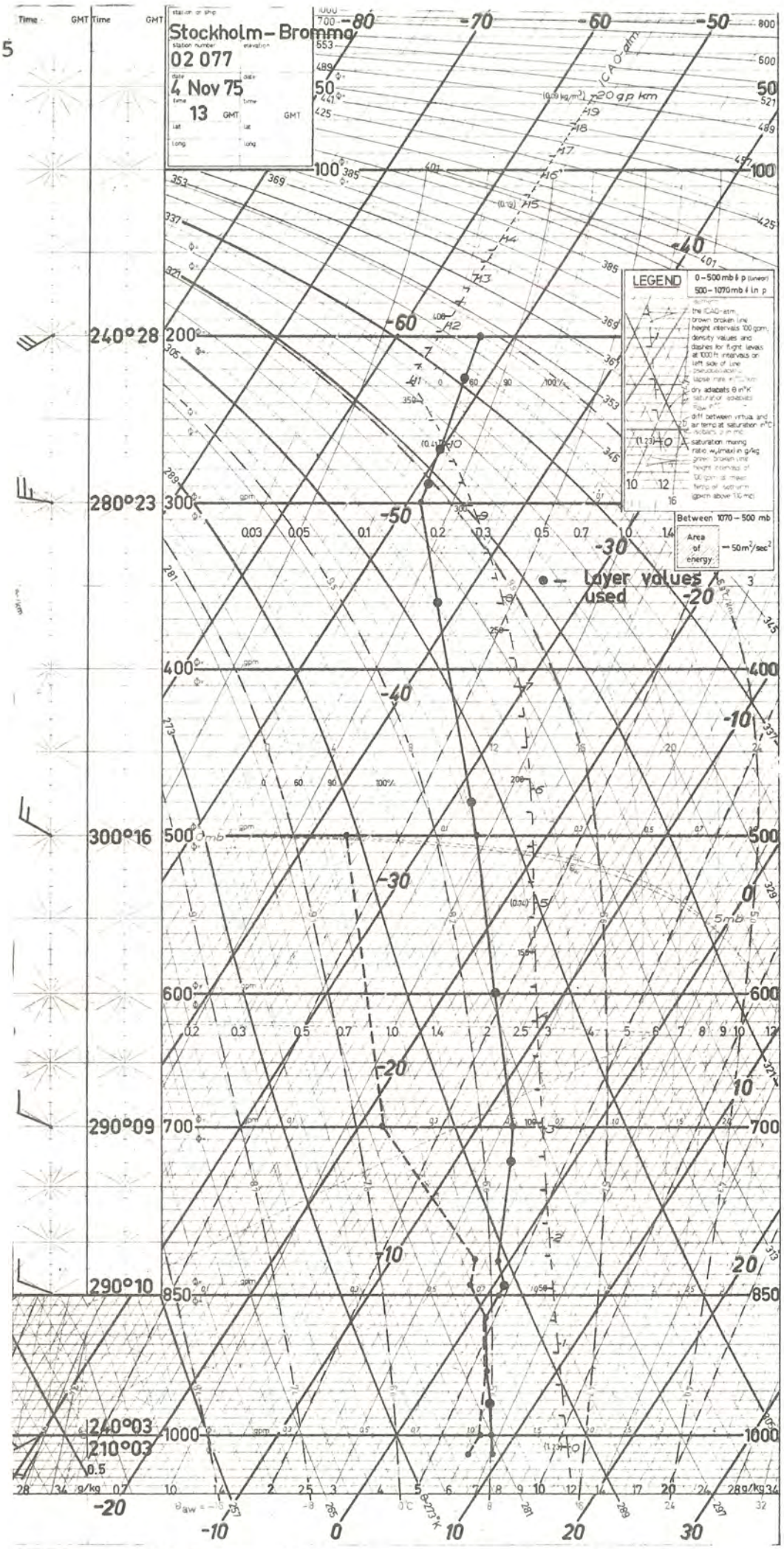

Figure 4. Stockholm-Bromma data, 4 Nov 1975 12Z, winds and temperatures. Layer values of temperature indicated by large dots.

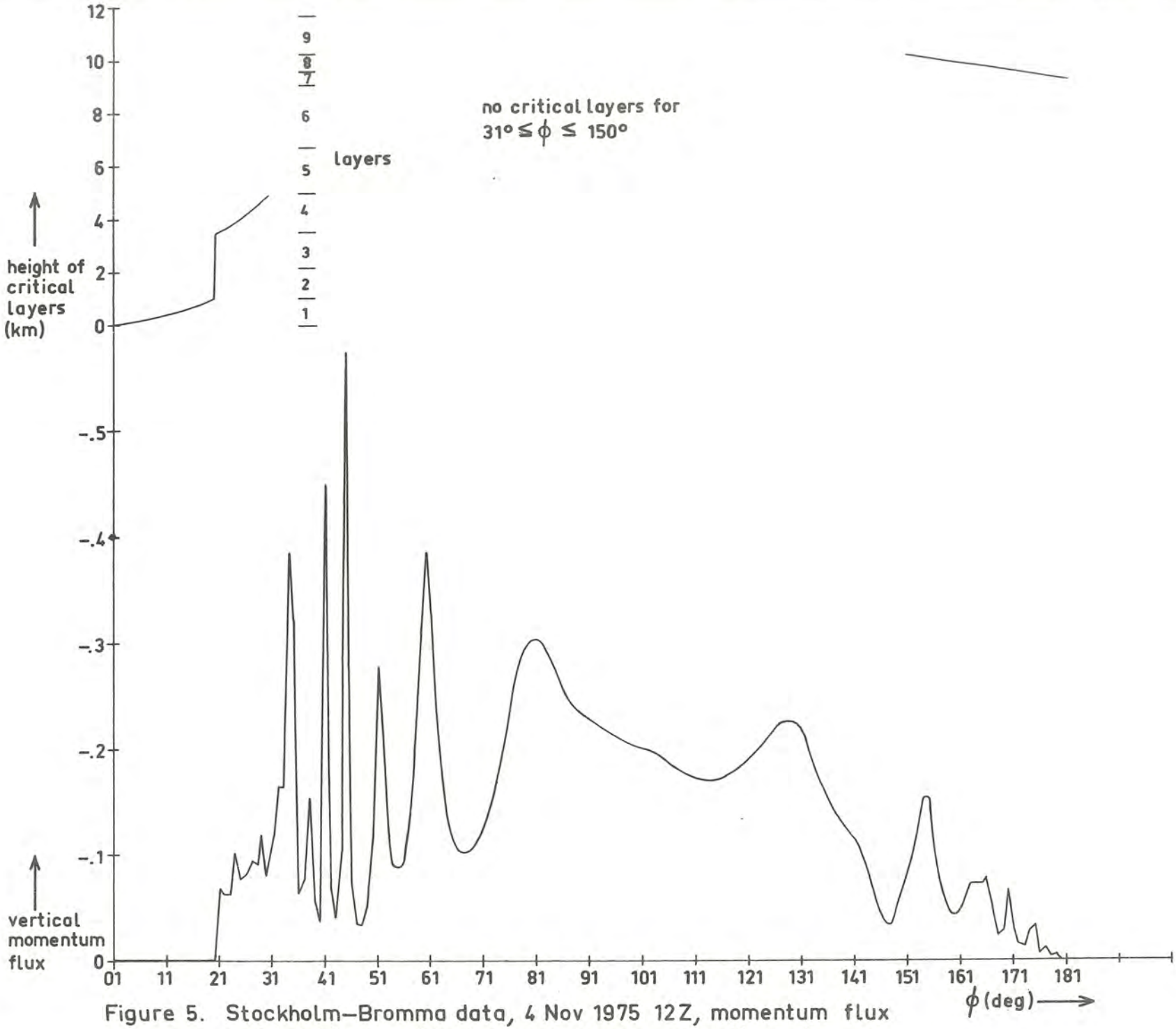

Figure 5. Stockholm–Bromma data, 4 Nov 1975 12Z, momentum flux and height of critical layers versus azimuth angle

Integration of the wave momentum fluxes with respect to azimuth shows about equal amounts of west and south-momentum absorbed within the model layers. In all, the absorbed momentum amounts to about 8% of the total vertical momentum flux. The implied large-scale wind tendencies are in the range of $1X10^{-5}$-$2.5X10^{-4}$ m/s^2 within layers having critical levels (layers 4,7, 8). The largest change is implied within the 8th layer. It amounts to a tendency of about -2m/s·day to the large-scale v.

The large changes of the vertical momentum flux with azimuth angle has been found to be caused by near-resonance modes of oscillation. They seem to be a common feature of models of more that two layers. The method of calculating them with sufficient accuracy is still open to investigation. However, it appears that calculation of the momentum flux at 5° degree intervals in azimuth is sufficient for the required numerical integrations.

IX Geographical Variation of Momentum Fluxes.

Streamfunction data from the SMHI 6-layer quasigeostrophic model have been used to define wind and temperatures over most of Europe for January 19, 1976, 00Z. Momentum fluxes and flux divergence have been calculated for the area for the pressure levels 1000-850 mb, 850-700 mb, 700-500 mb, 500-300 mb, and 300-200 mb. Figures 6 to 9 show the results of these calculations.

Figure 6 shows the 1000 mb streamfunction. A low was situated over the Atlantic with strong winds to the north of England. A ridge line passed through southern Europe, with a series of low centers through the Mediterranean and northeast. This case was investigated to see the relationship of the momentum fluxes to the meteorological patterns, and therefore real mountains were not used to specify $A(\phi)$ for each grid box, but rather, an average value for the whole earth has been used everywhere. Thus, there will not be any correlation of patterns to actual mountain features. It will be the me-

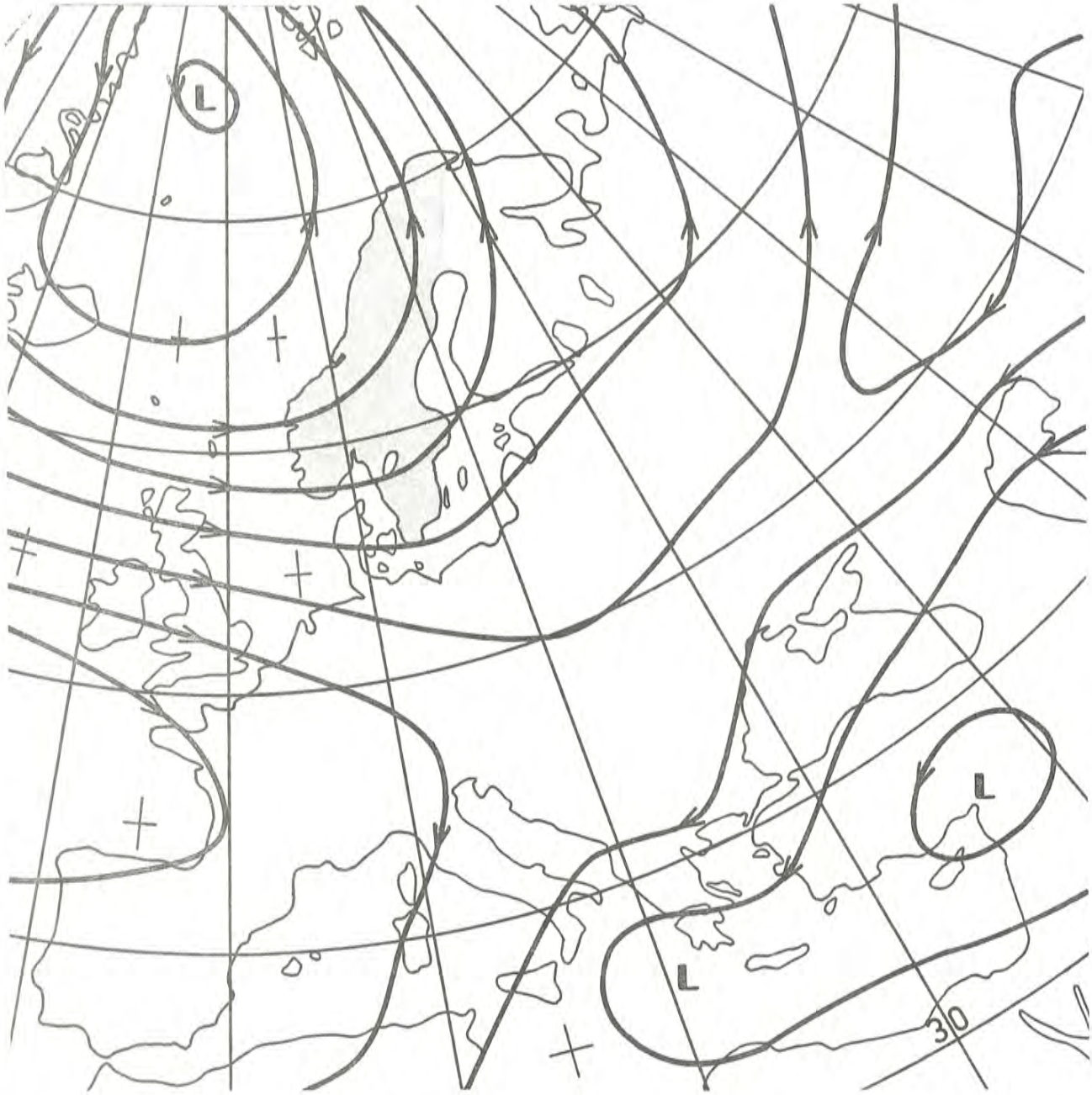

Figure 6.

1000 mb Streamfunction (5.0×10^6 m^2/s interval)

19 Jan 1976 00 Z

teorological patterns alone that determine the distribution of momentum fluxes and flux divergences. As such, we expect the generation of momentum flux to be largely correlated with the surface wind speed.

Figure 7 shows the 850 mb streams and the implied large-scale wind tendencies as a result of momentum flux divergence in the layer 850-700 mb. The largest values are in regions where the wind direction has changed from the surface direction as a result of baroclinicity.

Figure 8 shows the sum of the implied large-scale wind tendencies for the layers 850-700 mb, 700-500 mb, 500-300 mb, and 300-200 mb. The magnitudes are larger, but the pattern remains similar to that for the layer 850-700 mb. It is interesting to note that the flux divergence is relatively small over the strongest surface winds. This is true because the wind direction there changes little with height.

Figure 9 shows the 200 mb streamfunction field and the implied large-scale wind tendency above 200 mb. Here it is seen that there was indeed large momentum flux generation over the surface strong winds, but that it has passed up to the stratosphere, possibly affecting levels just above the jet.

X Discussion.

Additional calculations of momentum flux have been made for the January 19 case, but based upon a 6-hour forecast by the SMHI 6-layer quasi-geostrophic model from the initial data. Comparison of results shows relatively small changes, indicating temporal consistency of the wave flux calculations. Taken together with the fact that the wind tendencies as shown in figures 7 - 9 are in good relationship to the winds and their vertical direction changes, it is believed that the vertical momentum flux calculations have high credibility. In order to substantiate this statement, however, it will be necessary to make extensive and carefully designed experiments. The problem in determining

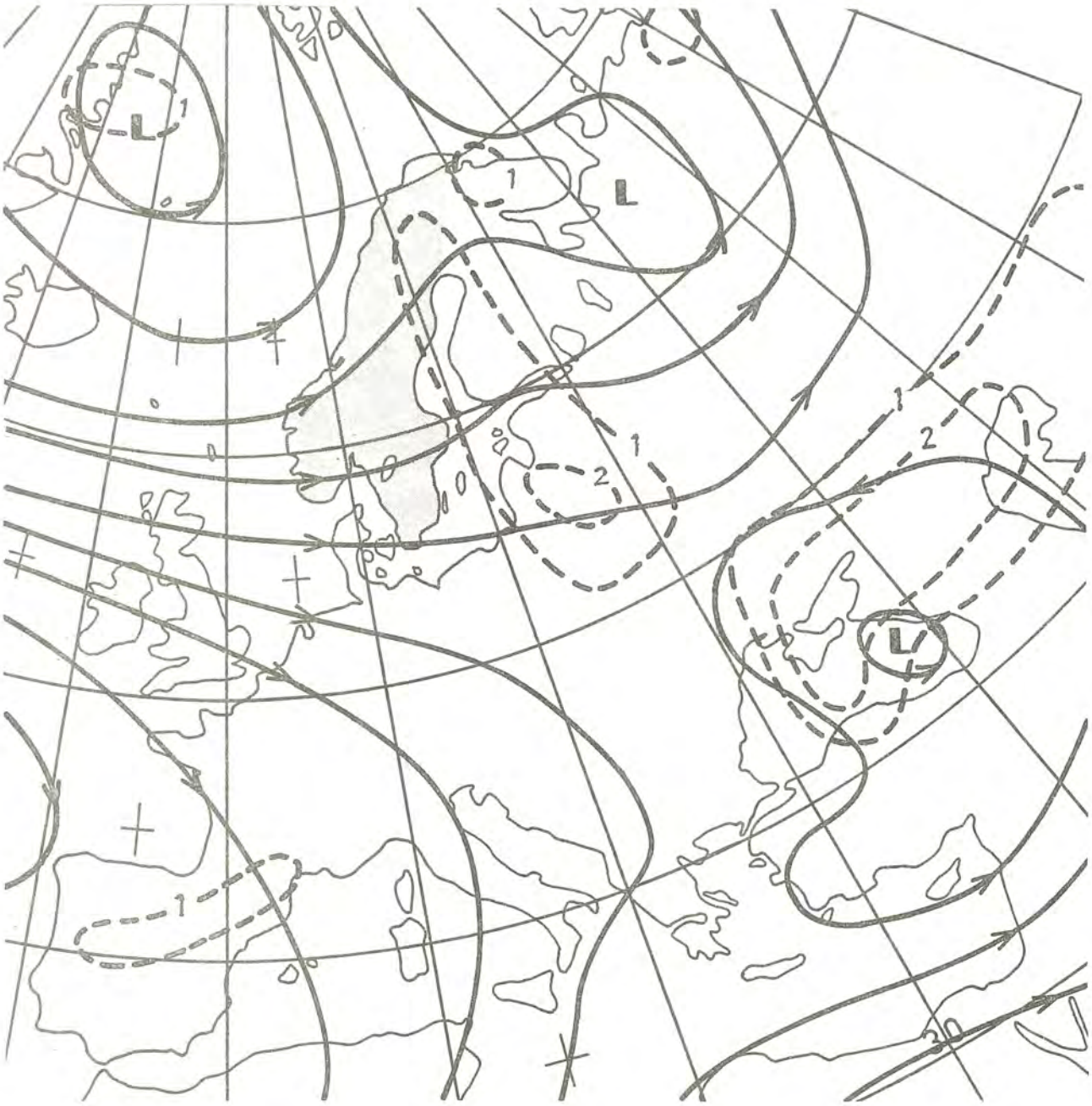

Figure 7.

850 mb Streamfunction (5.0×10^6 m^2/s interval) and

Wind tendencies, 850 –700 mb (m/s/day)

19 Jan 1976 00Z

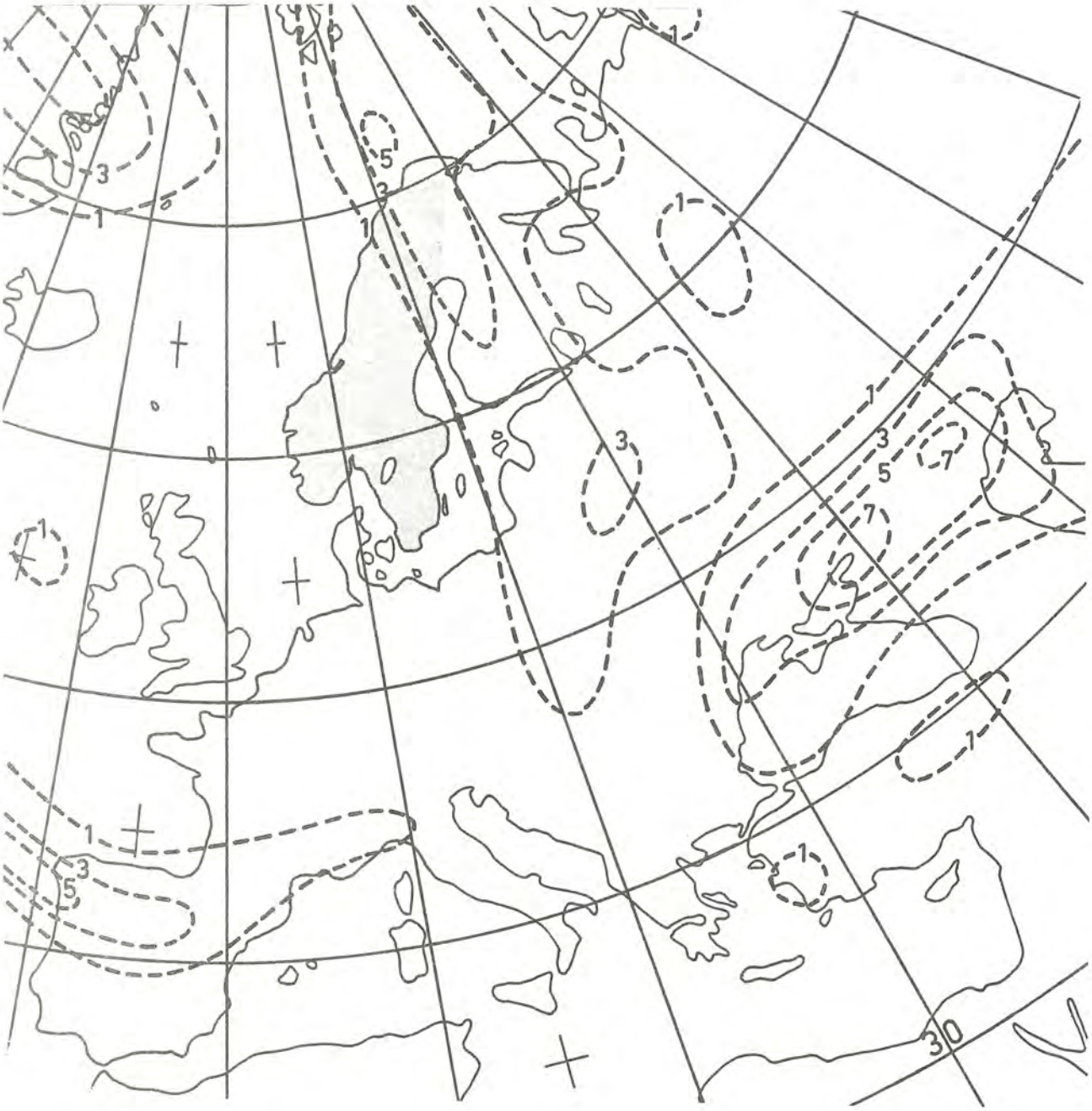

Figure 8.

Total of wind tendencies in layers (m/s/day)

850-700 mb

700-500 mb

500-300 mb

300-200 mb

19 Jan 1976 00Z

Figure 9.

200 mb Streamfunction (5.0×10^6 m^2/s interval) and

Wind tendencies, above 200 mb (m/s/day)

19 Jan 1976 00Z

the degree of validity of the calculations arises because they may not be compared with direct measurements except in perhaps a few isolated cases. And even in those cases, the observed values of momentum flux could easily be in error by a factor of two. Therefore, indirect methods of validation of the calculations must be made. An obvious method is the comparison of forecast model wind errors with the implied tendencies from vertical momentum fluxes. But such a comparison must be made carefully since model errors can be large and vary considerably from one model to another. A final method is to use the paramaterized wind tendencies in a large-scale model and see if any model improvement is obtained, particularly in mountaineous regions. But this method has most of the drawbacks of the last. It does provide one important piece of information, however. It provides a means of getting the benefit/cost ratio for a particular NWP model. This, of course, will determine whether the parameterization described in this note will be, in the final analysis, implemented.

Acknowledgements.

The author would like to thank the National Meteorological Center, Suitland, Maryland for supporting the research while on duty at the Swedish Meteorological and Hydrological Institute, Norrköping, Sweden. The author wishes to thank Mr. S. Bodin and Dr. I. Holmström for valuable discussions, Mrs. W. Böhm for drawing the figures and Mrs. K. Österlöf for typing the manuscript.

References

Benny, D J, and R F Bergeron, 1969, A new class of nonlinear waves in parallel flows., Studies in Appl Math, 48, pp 181-204.

Berkofsky, L, and E A Bertoni, 1960, Topographic charts at one-degree intersections for the entire earth., GRD Research Notes, No. 42, 43 pp.

Blumen, W, 1965, Momentum flux by mountain waves in a stratisfied, rotating atmosphere., JAS, 22, pp 529-534.

Booker, T R, and F P Bretherton, 1967, The critical layer for internal gravity waves in a shear flow, JF Mech, 27, pp 513-539.

Breeding, R T, 1972, A nonlinear model of the break-up of internal gravity waves due to their exponential growth with height, JGR, 11, No 15, pp 2681-2692.

Bretherton, F P, 1969, Momentum transport by gravity waves, GJRMS, 95, No 104, pp 213-243.

Bretherton, F P, 1971, GARP and clear air turbulence, Bull Amer Met Soc, 52, pp 17-21.

Bretherton, F P, 1966, The propogation of groups of internal gravity waves in shear flow, Quart J R Met Soc, 92, pp 466-480.

Eliassen, A, and E Palm, 1960, On the transfer of energy in stationary mountain waves, Geof Publ Oslo, 22, pp 1-23.

Hines, C O, 1960, Internal atmospheric gravity waves at ionospheric heights, Can J Phys, 38, pp 1441-1481.

Hines, C O, and Reddy, C A, 1967, On the propogation of atmospheric gravity waves through regions of wind shear, J Geophys Res, 72, pp 1015-1034.

Kelly, R E, and S A Maslowe, 1970, The nonlinear critical layer in a stably stratified shear flow. Studies in App Math, 49, pp 301-326.

Klemp, J B, and D K Lilly, 1975, The dynamics of wave-induced downslope winds, JAS, 32, pp 320-339.

Lee, W H K, and W M Kaula, 1967, A spherical analysis of the earth´s topography, JGR, 72, p 753.

Lilly, D, 1972, Wave momentum flux - a GARP problem, Bull Am Met Soc, 53, No 1, pp 17-23.

Lilly, D K, 1971, Observations of Mountain-Induced turbulence, JGR, 76, No 27, pp 6585-7688.

Lilly, D K, and P J Kennedy, 1973, Observations of a stationary mountain wave and its associated momentum flux and energy dissipation, JAS, 30, pp 1135-1152.

Lindzen, R S, 1973, Wave-mean flow interactions in the upper atmosphere. Boundary-Layer Meteor, 4, pp 327-343.

Maslowe, S A, 1972, Generation of clear air turbulence by non-linear waves. Studies in Appl Math, 51, pp 1-16.

Newton, C W, 1971, Mountain torques in the global angular momentum balance, JAS, 28, pp 623-628.

Orlanski, S, and K Bryan, 1969, Formation of thermocline step structure by large-amplitude internal gravity waves, JGR, 74, No 28, pp 6975-6983.

White, R M, 1949, The role of the mountains in the angular momentum balance of the atmosphere, J Met, 6, pp 353-355.

NOTISER OCH PRELIMINÄRA RAPPORTER, Serie METEOROLOGI

Nr 1 K a r l s s o n, K E, Instrumentala och visuella åskobservationer. (1960)

Nr 2 T h o m p s o n, T, Den naturliga radioaktivitetens variation med vädret. (1961)

Nr 3 M o d é n, H, Jämförelse mellan olika instrumentuppställning vid Gamla Observatoriet i Stockholm. (1963)

Nr 4 P e r s h a g e n, H, Snöförhållandenas svårighetsgrad under vintrarna 1931-1960 (1963)

Nr 5 M o d é n, H, Stockholms temperaturserie. (1963)

Nr 6 B e r g g r e n, R, En statistisk undersökning av vindriktningens vertikala variation i övre troposfären. (1963)

Nr 7 W a l l é n, C C, Sannolikheten för olika mängder av dygnsnederbörd i Sverige. (1963)

Nr 8 L i n d h o l m, F, Report on comparisons at Stockholm and Visby between the K Ångström original absolute scale and the new Smithsonian absolute scale for primary standard pyrheliometers. (1963)

Nr 9 M o d é n, H, Åskans dagliga period i Sverige. (1963)

Nr 10 Å n g s t r ö m, A, Some fundamental principles concerning calibration and standardization of pyrheliometers. (1964)

Nr 11 R o d h e, B, Comparison of pyrheliometers at different turbidity conditions. (1964)

Nr 12 S j ö l a n d e r, G, En statistisk undersökning av kuling och storm i svenska farvatten. Del 1, Västkusten norra delen. (1965)

Nr 13 T h o r s l u n d, B, Isförhållanden i svenska farvatten under normalperioden 1931-1960. (1966)

Nr 14 E r i k s s o n, B, Sannolikhetsfördelningar av temperatur, nederbörd och vind vid olika väderlekstyper. (1967)

Nr 15 T h o r s l u n d, B, Havsisens utbredning i Bottniska viken, Östersjön, Kattegatt och Skagerack under isvintrarna 1951/52-1966/67. (1967)

Nr 16 S c h m a c k e, E, Blixträkning med instrument. Synpunkter jämte preliminära resultat av timregistrering av blixtaktiviteten i södra Sverige under åren 1962-1966. (1968)

Nr 17 P o h l m a n, J, En statistisk undersökning av kuling och storm i svenska farvatten. Del 4, Farvattnen kring Gotland och norra Öland. (1968)

Nr 18 L u n d q v i s t, J-E, Isförhållanden i Vänern under perioden 1940-1963. (1969)

Nr 19 R o d h e, B, Comparison of the standard pyrheliometer Å 158 with the sub-standard instrument Å 70 and Å 171. (1969)

Nr 20 R o d h e, B, Simplified formulae for computation of the turbidity coefficient. (1969)

Nr 21 S a l o m o n s s o n, G, En statistisk undersökning av kuling och storm i svenska farvatten. Del 3, södra Östersjön. (1969)

Nr 22 H o l m s t r ö m, E, Extrapolation of meteorological data. (1969)

Nr 23 J o e l s s o n, R, Applicering av empiriska ortogonala funktioner på en synoptisk vädersituation. (1970)

Nr 24 L ö n n q v i s t, O, MASKINELL PROGNOSTEXT: Ett experiment med i datamaskin formulerade väderrapporter. (1971)

Nr 25 N y b e r g, A och H å r s m a r, P-O, Mätningar av avdunstning-kondensation samt snösmältning från en snöyta. (1971)

Nr 26 P e r s s o n, Anders O, En enkel metod att beräkna rådande vertikalvind och nederbördsintensitet ur aeorologiska vind- och fuktighetsdata. (1971)

Nr 27 H e n r i k s o n, A-B, An investigation of the accuracy in numerical computations of horizontal trajectories in the atmosphere. (1971)

Nr 28 A x e l s s o n, G, Studium av infraröda (IR) satellitfotografier mottagna vid SMHI vintern 1971 samt en resumé av indirekt bestämning av atmosfärens vertikala temperaturprofil med hjälp av strålningsdata från satelliter. (1971)

Nr 29 S c h m a c k e, E, FRÅN METEOROLOGINS GRYNING. Några drag i forntidens meteorologi. (1971)

Nr 30 L ö n n q v i s t, O, Några glimtar från Svensk klimatologi under 1700- och 1800-talet. (1972)

Nr 31 B l e c k e r t, G och M o e n, L, Meteorologisk ADB-verksamhet vid SMHI. (1972)

Nr 32 E r i k s s o n, B, Temperatur- och nederbördsförhållanden i Sverige 1961-70 i relation till perioden 1931-60. (1972)

Nr 33 B o d i n, S, A quasi-geostrophic 3-parameter numerical prediction model in empirical orthogonal functions. (1972)

Nr 34 R o d h e, B, The procedure of reading the Ångström Compensation Pyrheliometer. (1972)

Nr 35 J a k o b s o n, L, Verifikation av prognoser av dygnsmedeltemperaturen för Stockholmsområdet. (1973)

SMHI Rapporter, METEOROLOGI OCH KLIMATOLOGI (RMK)

Nr 1 T h o m p s o n, T, U d i n, I, och O m s t e d t, A, Sea surface temperatures in waters surrounding Sweden. (1974)

Nr 2 B o d i n, S, Development of an unsteady atmospheric boundary layer model. (1974)

Nr 3 M o e n, Lars, A multilevel quasi-geostrophic model for short range weather predictions. (1975)

Nr 4 H o l m s t r ö m, I, Optimization of atmospheric models. (1976)

Nr 5 C o l l i n s, William G, A PARAMETERIZATION MODEL FOR CALCULATION OF VERTICAL FLUXES OF MOMENTUM DUE TO TERRAIN INDUCED GRAVITY WAVES. (1976)